LAWRENCE
LIVERMORE
NATIONAL
LABORATORY

LLNL-JRNL-563558

A (S)TEM Gas Cell Holder with Localized Laser Heating for In-Situ Experiments

S. Mehraeen, J. T. McKeown, P. V. Deshmukh, J. E. Evans, P. Abellan, P. Xu, B. W. Reed, M. L. Taheri, P. E. Fischione, N. D. Browning

July 6, 2012

Microscopy and Microanalysis

Disclaimer

Atomic-resolution scanning transmission electron microscopy at atmospheric pressure

Shareghe Mehraeen[1,], Joseph T. McKeown[2,*], Pushkarraj V. Deshmukh[3], James E. Evans[1,4], Patricia Abellan[4], Pinghong Xu[5], Bryan W. Reed[2], Mitra L. Taheri[6], Paul E. Fischione[3], Nigel D. Browning[1,4,5]*

[1] Department of Molecular and Cellular Biology, University of California, Davis, CA 95616, USA

[2] Condensed Matter and Materials Division, Lawrence Livermore National Laboratory, Livermore, CA 94550, USA

[3] E.A. Fischione Instruments, Inc., Export, PA 15632, USA

[4] Chemical and Materials Science Division, Pacific Northwest National Laboratory, Richland, WA 99352, USA

[5] Department of Chemical Engineering and Materials Science, University of California, Davis, CA 95616, USA

[6] Department of Materials Science & Engineering, Drexel University, Philadelphia, PA 19104, USA

* Corresponding Author

Corresponding Author Email: smehraeen@gmail.com & mckeown3@llnl.gov

TABLE OF CONTENTS GRAPHIC

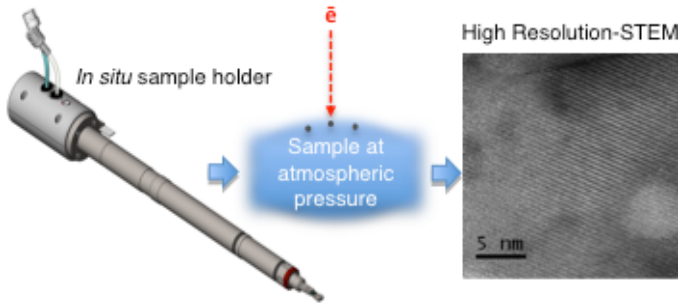

KEYWORDS: *in situ* gas holder; STEM; environmental microscopy; *in situ* microscopy, aberration correction

ABSTRACT

The advent of aberration correction for transmission electron microscopy has transformed atomic resolution imaging into a nearly routine technique for structural analysis. Now an emerging frontier in electron microscopy is the development of *in situ* capabilities to observe reactions at atomic resolution in real-time and within realistic environments. Here we present a new *in situ* gas holder that was designed to bypass several limitations that have plagued previous *in situ* gas holders. The new holder is compatible with any type of sample, and its capabilities include localized heating and precise control of the gas pressure and composition while simultaneously allowing atomic resolution imaging at ambient pressure. The results show that 0.25 nm lattice fringes are directly visible for nanoparticles imaged at ambient pressure with gas path lengths up to 20 μm. Additionally, we quantitatively demonstrate that while the attainable contrast and resolution decrease with increasing pressure and gas path length, resolutions better than 0.2 nm should be accessible at ambient pressure with gas path lengths less than the 15 μm utilized for these experiments.

The ability to study gas-solid interactions with atomic resolution and ambient pressures in the transmission electron microscope (TEM) promises new insights into the growth, properties, and functionality of nanomaterials. Heterogeneous catalysis is a particular application in which, the structure, morphology, and chemistry of nanoparticles are dynamic and greatly depend on the gas environment and temperature [1-7]. Unfortunately, conventional high-resolution TEM of catalysis is extremely challenging since both ambient pressure and elevated temperature can adversely affect imaging conditions. This is further complicated by the fact that normal TEM imaging is performed under a high vacuum ($1.5x10^{-7}$ Torr) to prevent unwanted scattering from gases. Therefore, to enable *in situ* experiments within the column of an electron microscope, a localized gas environmental chamber with controllable gas pressure, composition, and temperature is crucial. Such conditions can be obtained using an environmental cell built around the specimen.

The original designs for environmental cells have been around for over 70 years [8] and are produced by either incorporating differentially pumped apertures that separate the specimen from the high vacuum of the TEM column [1, 9-16] or windowed-cell designs that confine the gas within the specimen holder using electron-transparent membranes [4, 10, 17-22]. Atomic-resolution images in gaseous environments have been obtained with both techniques at pressures up to ~10 Torr [1, 5, 15, 22, 23], but the technological relevance of these measurements may not be compatible with the more realistic operating conditions of catalyst nanomaterials at higher pressures. Environmental transmission electron microscopes (ETEM) that incorporate differentially pumped apertures are generally limited to pressures of 15–20 Torr but they permit imaging a standard TEM sample. A windowed-cell approach produces a much thinner layer of gas (or fluid) than a differentially pumped ETEM and can examine samples at pressures greater than 50 Torr [10, 17]. However, the additional electron scattering due to the window membranes can decrease the attainable contrast and resolution. Recently, atomic-resolution imaging in a liquid environment was acquired at ambient pressure using a windowed-cell *in situ* liquid holder with fluid path lengths of 200–400 nm [24]. Unfortunately, such a thin path length for gaseous experiments

would only be amenable to nanoparticle research and not conventional dimpled and ion milled specimens.

While atomic-resolution *in situ* gas TEM has been previously demonstrated using a windowed-cell approach at atmospheric pressure and temperatures up to 500°C [17], many reactions, including those involving catalysts, require a greater temperature range. Additionally, the micromachined devices used in previous designs [17] heat the entire window surface and simultaneously react every nanoparticle. A direct heating source that is smaller than the windowed area and translatable across the surface would allow experiments to be imaged under equivalent conditions but at separate times to improve reproducibility. Possibilities for such localized heating could incorporate a partitioned micromachined device or focused laser. A new environmental-cell design using windowed cells with a variable gas path length is therefore critically needed to permit *in situ* observations of any type of sample at ambient pressure and elevated temperature in a manner that allows atomic resolution and statistical measurements through targeted heating and imaging.

Atomic-scale imaging of catalysts and other nanoparticles would also benefit from *in situ* aberration corrected high-angle annular dark-field Scanning TEM (HAADF-STEM) imaging [25]. This imaging mode can provide directly interpretable atomic-scale images of catalyst nanoparticles at the required pressures and temperatures. HAADF-STEM imaging is produced from incoherent, Rutherford-like scattering of electrons to high angles by the atomic nuclei of the specimen. The intensity (contrast) in the images is related to both the density and thickness (mass-thickness contrast) and the atomic number of the species responsible for scattering (typically referred to as Z-contrast imaging), generating images that reveal chemical information as well as structural information without potentially unwanted diffraction contrast [26-28]. This makes HAADF-STEM imaging ideal for catalysis studies in which small particles or clusters of heavy atoms sit on a substrate and it is necessary to differentiate chemically inhomogeneous structures at small spatial scales [29-32]. Recently, an edge resolution of 0.4 nm was reported for gold nanoparticles at ambient gas pressure using a windowed-cell holder in an uncorrected scanning TEM [33], but atomic lattice fringes were not observed. However, the use of an aberration-

corrected STEM can significantly improve the resolution by producing a smaller electron probe (<1 Å in some instances) relative to an uncorrected STEM, as the dark-field resolution is largely determined by the probe diameter.

Here, we demonstrate the capabilities of a new *in situ* holder capable of precisely controlling gas composition and pressure. The new holder has the ability to image any type of sample since the gas path length is adjustable between 0 and 250 μm and enables access to experiments at temperatures beyond the previous limitation of 500°C by incorporation of localized specimen heating using a translatable fiber-based laser. In this paper, we present atomic-resolution images obtained with aberration-corrected HAADF-STEM from two distinct experiments using nanoparticle specimens (TiO_2 and PbO). The images were acquired at ambient temperature and a range of pressures up to 800 Torr. Finally, we evaluate the effect of gas pressure on attainable resolution.

RESULTS

The design of the *in situ* environmental heating holder (E.A. Fischione Instruments, Inc.) employed in these studies incorporates a windowed environmental cell (e-cell) with a total height of 2 mm that makes it compatible with the objective pole pieces of most commercially available TEMs [34]. A pair of 15-nm-thick amorphous silicon nitride windows (Ted Pella, Inc.) created the electron-transparent reaction chamber as shown in Figure 1A&B. The e-cell is designed to accept a standard 3-mm-diameter TEM specimen and a modular design allows for a variation in the spacer height and gas path length (GPL) to accommodate various sample thicknesses up to 250 μm. The modular spacers consist of 15-μm-thick titanium discs with an outer diameter of 3 mm and an inner diameter of 1 mm to provide a gap between the two silicon nitride membranes for gas flow in and out of the e-cell without obscuring the viewable area. For the experiments described here, nanoparticles were placed directly on the inner side of the upper membrane (entrance window with respect to the scanning electron probe) of the e-cell to minimize probe broadening prior to scattering by the specimen.

Figure 1C shows a schematic of the complete gas-flow assembly. This design has the provision of flowing up to four different gases simultaneously through the cell. The gas flow is controlled accurately using pressure regulators and mass flow controllers. The gases initially flow into a mixing chamber external to the TEM, and from there the gas mixture is circulated into the specimen chamber of the holder through the inlet port. Pressure gauges at the inlet and outlet ports are used to determine the average steady-state pressure within the e-cell. Simultaneous pumping of the e-cell with an external two-stage diaphragm and turbomolecular pump and/or regulating the mass flow rate of the gases can accurately vary the pressure inside the e-cell. All flow regulations are computer controlled using a LabVIEW™ interface.

The new holder also incorporates a built-in laser optics assembly to focus an infrared laser onto the specimen for localized heating experiments. The laser enters the end of the holder via a fiber optic cable and is focused onto the sample using a 60° titanium mirror with 5 nm gold plating. The optics are adjustable to yield a spot size on the sample between 30 and 300 μm and translatable along the sample plane x- and y-axes. Figure 2 shows bright field TEM images of hollow zinc oxide nanoparticle generation from a core-shell zinc/zinc oxide (Zn/ZnO) nanoparticle following infrared heating. Power spectra of the amorphous SiN membrane to which the nanoparticles are attached show that the images were acquired at the same focus, indicating the contrast change is not due to defocus effects. At a laser power setting of 18% and a spot size of 200 μm (power density of 4.9×10^7 W/m^2), the solid zinc core disappears leaving behind a zinc oxide shell as a hollow nanoparticle. Similar results were achieved during previously published *ex situ* laser heating experiments [35] where hollow ZnO nanoparticles were formed following selective-laser vaporization of Zn/ZnO core shell nanoparticles. The vaporization of the solid core occurs when the nanoparticle is heated (with a laser photon energy below the band gap of the shell material) to a temperature above the core material boiling point but below the shell material melting point. For the Zn/ZnO nanoparticle shown in Figure 2, this corresponds to a temperature above 907°C but below 1975°C [35]. To verify that the ZnO shell did not expand during this experiment while the Zn core disappeared, we included line profiles for equivalent regions of the nanoparticle before and

after heating (Figure 2C-F). Since we systematically increased the laser temperature to achieve these results we are confident that we are above 907°C, but we are not sure of the deviation above this value. A more detailed analysis using multiple samples (of similar size and shape) and data points will be needed to fully calibrate a plot for laser power versus sample temperature. Based on these results, it would be theoretically possible to achieve a local sample temperature greater than 10,000°C with this holder if the power density was increased to 50% and the spot size decreased to 100 μm (assuming a linear effect and a similar sample absorption rate of 40% [36]. However, a maximum operating value of 2000°C is more realistic for this *in situ* gas holder. This temperature limit would avoid thermal radiation from the sample compromising the integrity of the silicon nitride membrane and gold plating on the mirror. Although the higher temperature capabilities of the holder are the focus of a separate paper, the possibility of achieving localized sample temperatures up to 2000°C will permit imaging of many high-temperature catalyst systems currently not amenable to *in situ* analysis.

As a first test specimen for verifying the resolution achievable with HAADF-STEM and the new *in situ* gas holder under atmospheric conditions we imaged PbO nanoparticles directly attached on the inner side of the upper membrane. Figure 3 shows raw images of PbO recorded at 20 and 800 Torr (>1 atm) along with respective direct Fourier Transforms (FT). Lattice fringes at 0.25 nm are visible in the images of PbO nanoparticles at all applied pressures up to 800 Torr (average steady-state). However, while we detected 0.18 nm fringes while imaging particles at 20 Torr none of the particles imaged at 800 Torr depicted fringes beyond 0.2 nm. This could of course be due to the orientation of the nanoparticles during imaging or it could be due to an adverse effect for resolution dependent on gas pressure, path length, and/or membrane thickness.

Any loss of resolution due to increasing the gas pressure to 800 Torr can be explained by plural scattering from a combined effect of the silicon nitride membranes and gas molecules. Unlike standard imaging where the sample is exposed to the vacuum of the microscope, *in situ* e-cell imaging (both gas and liquid environments) involves extra material density surrounding the sample of interest which causes plural scattering and can degrade image contrast and resolution. Additionally, this effect gets

worse as the pressure increases due to outward membrane bulge that results in a larger gas path length. However, the magnitude of resolution loss is dependent on where the sample is located relative to the upper membrane. With the sample adhered to the opposite (bottom) window, the scanned probe is broadened due to scattering caused by interaction of the electron beam with the upper window and the density of gas molecules prior to surveying the sample. Since the resolution in HAADF-STEM is dependent on the probe size, this type of broadening directly limits the attainable resolution. During these experiments we were unable to detect any lattice fringes for nanoparticles on the bottom window. On the other hand, when the particles are attached to the upper membrane, the scattering from the gas density occurs after the electrons have already interacted with the specimen and decreases the signal to background ratio. This is because some electrons that would have hit the HAADF detector will be randomly scattered away from it and vice versa. Thus, there may be some critical pressure, GPL, and/or density beyond which atomic lattice fringes for a given resolution will no longer be observed as the noise effectively blurs the lattice fringes.

For our experiments, the initial GPL was nominally set with a single 15 μm titanium spacer inserted between the upper and the lower silicon frames. When the e-cell was pressurized, the silicon nitride membranes bulged due to the pressure differential between the e-cell and vacuum of the microscope column and the bulging was measured experimentally by calculating the change in eucentric height position of each membrane as the pressure inside the e-cell increased. While the GPL at the edge of the windowed area matched the nominal spacing of 15 μm, the middle of the window bulged to a gas path length of ~50 μm at 760 Torr. Using the approach of Creemer *et al.* [37], we calculated the atomic density projected along the path of the electron beam through the gas by integrating the molecular density through the thickness of the environmental cell (there will be contributions from both the window membranes and the gas). For O_2 gas at 760 Torr and 300°K with a 50 μm gas path length, this gives a projected density of ~2.5×10^3 atoms/nm^2 due to the gas molecules only. This projected gas density matches the density previously obtained both in a nanoreactor with H_2 gas at ~750 Torr (34 μm GPL and 0.18 nm resolution) and in an ETEM with N_2 gas at ~4 Torr (5 mm GPL and 0.14-nm

resolution) [38]. Interestingly, atomic resolution was not obtained in the present experiments when the gas path length was 50 μm for particles on the upper window. Instead, a critical path length of less than 20 μm was required to observe lattice fringes at 760 Torr and above. Taking into account the contribution from the 15-nm-thick nitride membranes, this corresponds to a critical projected atomic density of ~7×10^3 atoms/nm^2 (~1×10^3 atoms/nm^2 are due to the gas molecules). Since each silicon nitride membrane contributes $3x10^3$ atoms/nm^2 in the projected atomic density, scattering from the membranes is currently much stronger than the scattering from the gas molecules. As a result using thinner membranes would likely permit even higher resolution imaging conditions than presented here, however a simultaneous decrease in window areas will be required to maintain sufficient mechanical resistance to the differential pressure experienced by the e-cell during loading into the microscope.

To verify these results and test the versatility of combining the *in situ* holder with HAADF-STEM for imaging nanoparticles composed of lower atomic number elements, a titanium (IV) oxide (TiO_2) nanopowder with an average particle size of ~25 nm was also imaged. Figure 4 shows atomic-resolution HAADF-STEM images of TiO_2 nanoparticles at four pressures ranging from the vacuum of the microscope column (~10^{-7} Torr) to 760 Torr. To quantify the resolution loss as a function of pressure, we analyzed line profiles and Bragg spot intensities corresponding to the 0.25 nm lattice fringes from the nanoparticles shown in Figure 4A-D. Since the membrane thickness used for these images were identical, the images were shifted to an equivalent average pixel value for the amorphous SiN background prior to calculating the line profiles. This constant adjustment of pixel values generated a relative reference value from which the effect of pressure on resolution could be assessed. As seen in Figure 4E, the average signal levels of the particles and background were similar for both the 40 and 760 Torr images. However, the peak-to-valley height for the 0.25 nm lattice fringes at 760 Torr was roughly 33% of the height at 40 Torr. The decrease in fringe visibility with increasing pressure was validated by a second measurement of Bragg spot intensity quotient (IQ) values. To calculate the IQ values, direct Fourier Transforms of the images were performed and the central peak intensity of each Bragg spot was compared to the average intensity of background pixels. To ensure the background

pixels were representative and did not include above-average intensity due to a broadened spot, a radius of 10 pixels from the central peak was used to calculate the average background value (excluding all values within 9 pixels of the central peak). Figure 4F depicts a plot of the IQ values normalized to the IQ value calculated at 40 Torr. The plot indicates a decrease of spot intensity at 760 Torr to 72% of the intensity at 40 Torr. It is important to note that the line profile analysis is an absolute measure while the IQ analysis is a relative measure of contrast. The IQ analysis has been used for over 25 years in the biological TEM community where it was developed to evaluate images with low signal-to-noise levels [39]. Although the doses used here were higher than the typical low-dose images of biological TEM, the IQ analysis provided a convenient mechanism for qualitatively comparing the different imaging conditions due to varying pressure. Bragg spots can be detected in the power spectrum of an image even when the particle contrast is nearly zero. Thus despite the discrepancy in magnitude between the two measurements appearing large, both analysis methods support a significant loss of contrast and resolution as a function of pressure. The observation that the 0.18 nm fringes were absent in images acquired at ambient pressure (while the 0.25 nm fringes remained visible) suggests that plural scattering limited the resolution to around 0.2 nm for the microscope and holder assembly conditions utilized during these experiments. Since the increase in gas pressure was accompanied by window bulging as described above, we could not fully determine if the resolution loss was due to the change in pressure or gas path length. However, since both variables affect the total number of gas molecules that reside in the path of the electron beam and cause plural scattering, the use of a thinner nominal path length than the 15 μm spacer used here may permit imaging on the 1-angstrom scale for future experiments.

DISCUSSION

The results presented here demonstrate that aberration-corrected atomic-resolution HAADF-STEM images can be obtained from nanoparticles at technologically relevant pressures greater than 760 Torr. The new *in situ* gas holder design bypasses previous limitations with sample flexibility, localized heating, and large field of view. Optimization of the parameters required for atomic-resolution STEM

imaging in ambient pressures involved overcoming several multifaceted challenges in design, engineering, and experimental planning such as specimen drift, carbon contamination, and blurring factor of the windows. The first results of these efforts are presented here as an initial step toward developing a technique capable of creating a realistic environment (ambient pressures and elevated temperatures) in an electron microscope for *in situ* studies of catalytic materials on substrates.

Recently, Electron Energy Loss Spectroscopy has been demonstrated for ambient pressure *in situ* liquid studies [40] and could potentially be combined with the holder described here to track the electronic states of catalyst particles and clusters at elevated pressures and temperatures while the structure and morphology are monitored with HAADF-STEM imaging. Extending these experimental capabilities further to techniques that employ high temporal resolution such as Dynamic TEM [41] could potentially allow observation of transient states of catalysts while also providing the added benefit of overcoming drift due to specimen heating. The ability to couple these novel platforms for *in situ* analysis using this new environmental cell opens up a large number of possibilities to study functional nanomaterials under relevant ambient conditions.

METHODS

Nanoparticle Preparation: The PbO nanoparticles were grown by first forming lead sulfide nanoparticles in solution [24] followed by deposition on the window surface and oxidation at room temperature [42]. The TiO_2 nanopowder (Sigma Aldrich®, ≥99.5% pure titanium (IV) oxide, 25 nm) and Zn nanoparticles (Sky Spring Nanomaterials, 99.9% zinc, 80–100 nm) were used as purchased and deposited directly on the window surface prior to imaging. In the case of the Zn nanoparticles, the exposure to air during loading of the holder resulted in the formation of a zinc oxide shell surrounding the Zn core.

Scanning Transmission Electron Microscopy and In Situ Imaging: HAADF-STEM imaging with the *in situ* holder was performed in an aberration-corrected JEOL JEM-2100F/Cs operating at 200 keV using a

probe current of ~72 pA and a dwell time of 15 μs/pixel. TEM imaging was performed in an aberration-corrected JEOL JEM-2200F, also operated at 200 keV. All *in situ* images were recorded in O_2 gas with >99.5% purity, as this provides a means of removing hydrocarbon contamination that may develop during experiments [19]. For the heating experiment, a 1085 nm laser (total power output of 8.5 W) was operated at 18% power with a sample plane spot size of 200 μm providing a power density at the sample of 4.9×10^7 W/m^2.

ACKNOWLEDGEMENTS

Development of the *in situ* holder was supported by DOE NNSA-SSAA grant number DE-FG52-06NA26213 and NIH grant number RR025032-01. J.E. acknowledges NIH funding support from grant number 5RC1GM091755. A portion of this work was performed at the Pacific Northwest National Laboratory, which is operated by Battelle Memorial Institute for the U.S. Department of Energy under Contract No. DE-AC05-76RL01830. A portion of this work was performed at the Lawrence Livermore National Laboratory and supported by the Office of Science, Office of Basic Energy Sciences, Division of Materials Science and Engineering of the U.S. Department of Energy under Contract No. DE-AC52-07NA27344.

REFERENCES

1. Boyes, E. D.; Gai, P. L. *Ultramicroscopy* **1997,** 67, 219-32.

2. Chang, L.-Y.; Barnard, A. S.; Gontard, L. C.; Dunin-Borkowski, R. E. *Nano Letters* **2010,** 10, 3073-76.

3. Gai, P. L.; Boyes, E. D.; Helveg, S.; Hansen, P. L.; Giorgio, S.; Henry, C. R. *Materials Research Bulletin* **2007,** 32, 1044-50.

4. Giorgio, S.; Joao, S. S.; Nitsche, S.; Chaudanson, D.; Sitja, G.; Henry, C. R. *Ultramicroscopy* **2006,** 106, 503-7.

5. Hansen, P. L.; Wagner, J. B.; Helveg, S.; Rostrup-Nielsen, J. R.; Clausen, B. S.; Topsoe, H. *Science* **2002,** 295, 2053-55.

6. Ueda, K.; Kawasaki, T.; Hasegawa, H.; Tanji, T.; Ichihashi, M. *Surface and Interface Analysis* **2008,** 40, 1725-27.

7. Wang, R.; Crozier, P. A.; Sharma, R. *Journal of Physical Chemistry C* **2009,** 113, 5700-4.

8. Marton, L. *Bulletin de la Classe des Sciences Academie Royale de Belgique* **1935,** 21, 553-64.

9. Baker, R. T. K.; Harris, P. S. *Journal of Physics E* **1972,** 5, 793-97.

10. Butler, E. P.; Hale, K. F., *Dynamic Experiments in the Electron Microscope*. North-Holland Publishing Group: Amsterdam, 1981; Vol. 9.

11. Lee, T. C.; Dewald, D. K.; Eades, J. A.; Robertson, I. M.; Birnbaum, H. K. *Review of Scientific Instruments* **1991,** 62, 1438-44.

12. Robertson, I. M.; Teter, D. *Microscopy Research and Technique* **1998,** 42, 260-69.

13. Sharma, R. *Microscopy and Microanalysis* **2001,** 7, 494-506.

14. Sharma, R. *Journal of Materials Research* **2005,** 20, 1695-707.

15. Sharma, R.; Weiss, K. *Microscopy Research and Technique* **1998,** 42, 270-80.

16. Zhang, M.; Olson, E. A.; Twesten, R. D.; Wen, J. G.; Allen, L. H.; Robertson, I. M.; Petrov, I. *Journal of Materials Research* **2005,** 20, 1802-7.

17. Creemer, J. F.; Helveg, S.; Hoveling, G. H.; Ullmann, S.; Molenbroek, A. M.; Sarro, P. M.; Zandbergen, H. W. *Ultramicroscopy* **2008,** 108, 993-98.

18. Daulton, T. L.; Little, B. J.; Lowe, K.; Jones-Meehan, J. *Microscopy and Microanalysis* **2001,** 7, 470-85.

19. Heide, H. G. *Journal of Cell Biology* **1962,** 13, 147-52.

20. Komatsu, M.; Mori, H. *Journal of Electron Microscopy* **2005,** 54, 99-107.

21. Konishi, H.; Ishikawa, A.; Jiang, Y.-B.; Buseck, P.; Xu, H. *Microscopy and Microanalysis* **2003,** 9, 902-3.

22. Parkinson, G. M. *Catalysis Letters* **1989,** 2, 303-7.

23. Helveg, S.; López-Cartes, C.; Sehested, J.; Hansen, P. L.; Bjerne, S. C.; Rostrup-Nielsen, J. R.; Abild-Pederson, F.; Nørskov, J. K. *Nature* **2004,** 427, 426-29.

24. Evans, J. E.; Jungjohann, K. L.; Browning, N. D.; Arslan, I. *Nano Letters* **2011,** 11, 2809-13.

25. Nellist, P. D.; Chisholm, M. F.; Dellby, N.; Krivanek, O. L.; Murfitt, M. F.; Szilagyi, Z. S.; Lupini, A. R.; Borisevich, A.; Sides Jr., W. H.; Pennycook, S. J. *Science* **2004,** 305, 1741.

26. Crewe, A. V.; Isaacson, M.; Johnson, D. *Review of Scientific Instruments* **1969,** 40, 241.

27. Crewe, A. V.; Wall, J.; Langmore, J. *Science* **1970,** 168, 1338.

28. Pennycook, S. J. *Ultramicroscopy* **1989,** 30, 58.

29. Howie, A.; Marks, L. D.; Pennycook, S. J. *Ultramicroscopy* **1982,** 8, 163.

30. Pennycook, S. J. *Journal of Microscopy* **1981,** 124, 15.

31. Pennycook, S. J.; Howie, A.; Shannon, M. D.; Whyman, R. *Journal of Molecular Catalysis* **1983,** 20, 345.

32. Treacy, M. M. J.; Howie, A.; Wilson, C. J. *Philosophical Magazine A* **1978,** 38, 569.

33. de Jonge, N.; Bigelow, W. C.; Veith, G. M. *Nano Letters* **2010,** 10, 1028-31.

34. Deshmukh, P. V.; Gronsky, J. J.; Fischione, P. E. In Situ Holder Assembly. 2012.

35. Niu, K. Y.; Yang, J.; Kulinich, S. A.; Sun, J.; Du, X. W. *Langmuir* **2010,** 26, 16652-57.

36. Bergström, D.; Powell , J.; Kaplan, A. F. H. *Applied Optics* **2007,** 46, 1290-1301.

37. Creemer, J. F.; Helveg, S.; Kooyman, P. J.; Molenbroek, A. M.; Zandbergen, H. W.; Sarro, P. M. *Journal of Microelectromechanical Systems* **2010**, 254-64.

38. Hansen, P. L.; Helveg, S.; Datye, A. K. *Advances in Catalysis* **2006,** 50, 77-95.

39. Henderson, R.; Baldwin, J. M.; Downing, K. H.; Lepault, J.; Zemlin, F. *Ultramicroscopy* **1986,** 19, 147–178.

40. Jungjohann, K. L.; Evans, J. E.; Aguiar, J.; Arslan, I.; Browning, N. D. *Microscopy and Microanalysis* **2012,** 18, 621 – 627.

41. Browning, N. D.; Bonds, M. A.; Campbell, G. H.; Evans, J. E.; LaGrange, T.; Jungjohann, K. L.; Masiel, D. J.; McKeown, J.; Mehraeen, S.; Reed, B. W.; Santala, M. *Current Opinions in Solid State and Materials Science* **2012,** 16, 23-30.

42. Zingg, D. S.; Hercules, D. M. *Journal of Pyhsical Chemistry* **1978,** 82, 1992-95.

FIGURES AND FIGURE LEGENDS

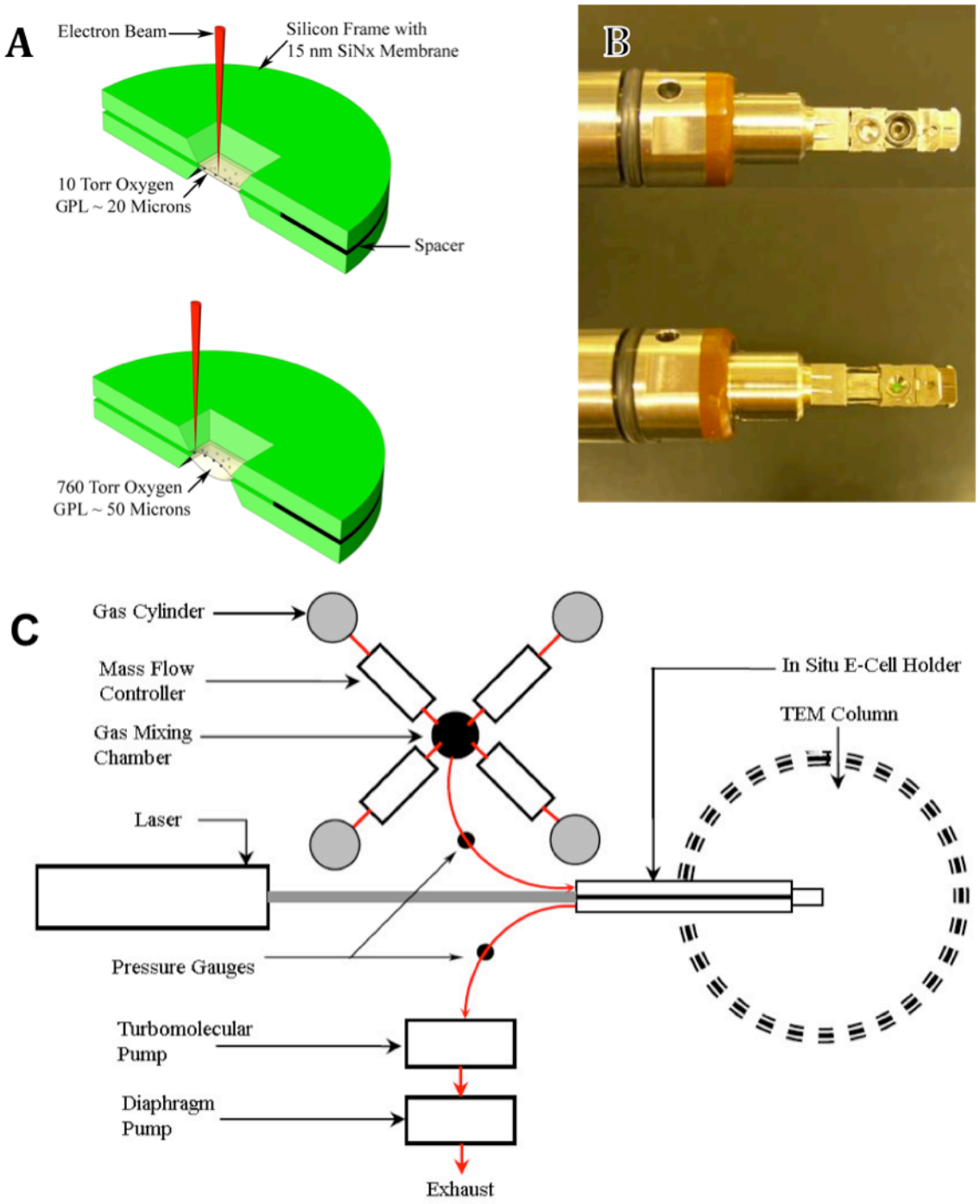

Figure 1: Overview of environmental gas flow holder design. A) Illustration showing a cross-section of the environmental cell at both low pressure (10 Torr) and atmospheric pressure (760 Torr). The silicon nitride membranes bulge as the pressure increases, resulting in a larger gas path length for scattered electrons. Nanoparticles are placed directly on the inner side of the upper window, as shown. B) The tip

of the *in situ* holder before mounting the windows (top) and after inserting the windows and securing the clamp to seal the chamber (bottom). C) Schematic view of the complete gas flow assembly.

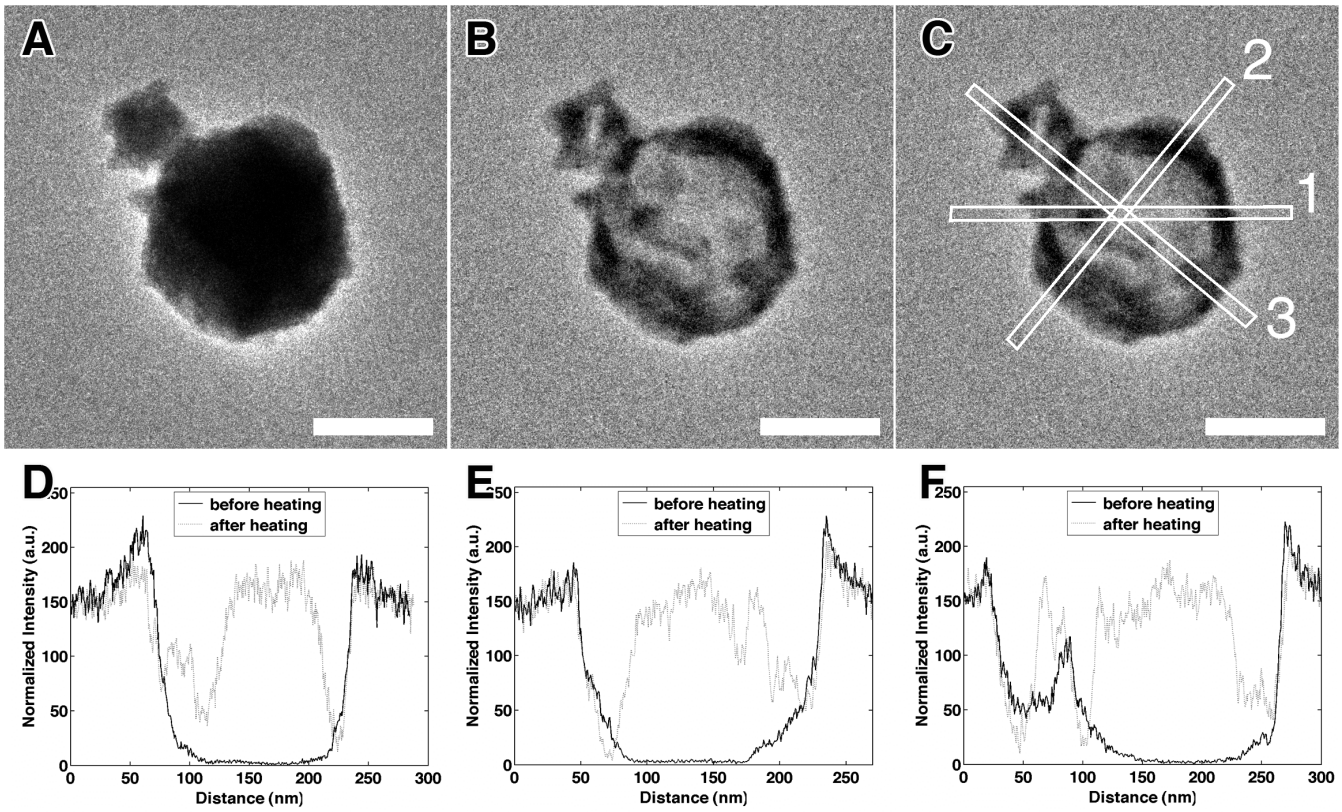

Figure 2: Generation of hollow zinc oxide nanoparticle using localized infrared laser heating. A) Zn/ZnO core-shell nanoparticle imaged at room temperature. B) Same particle as (A) following exposure to a 200 μm diameter continuous 1085 nm laser for 15 seconds with a power density of 4.9×10^7 W/m^2. Only the hollow ZnO shell remains. The scale bar is equivalent for both panels and represents 100 nm. C) Illustration showing the equivalent line scan regions for the particles shown in (A) and (B). Line scans 1-3 correspond to panels (D-F) respectively. All line scans depict the 20-pixel wide integrated profile before and after heating.

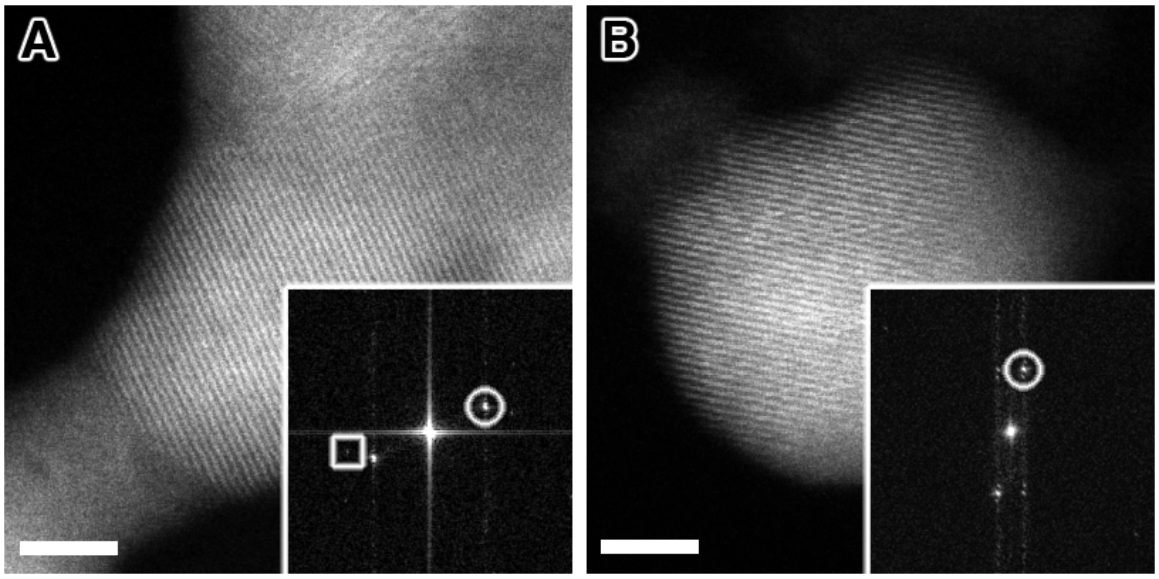

Figure 3: Atomic-scale resolution under gas flow. PbO nanoparticles showing atomic lattice fringes at A) 20 Torr and B) 800 Torr O_2 gas. FT insets show 0.25-nm lattice fringes (white circles) corresponding to (002) lattice planes and the 0.18 nm lattice fringes (white square). Scale bars represent 3 nm.

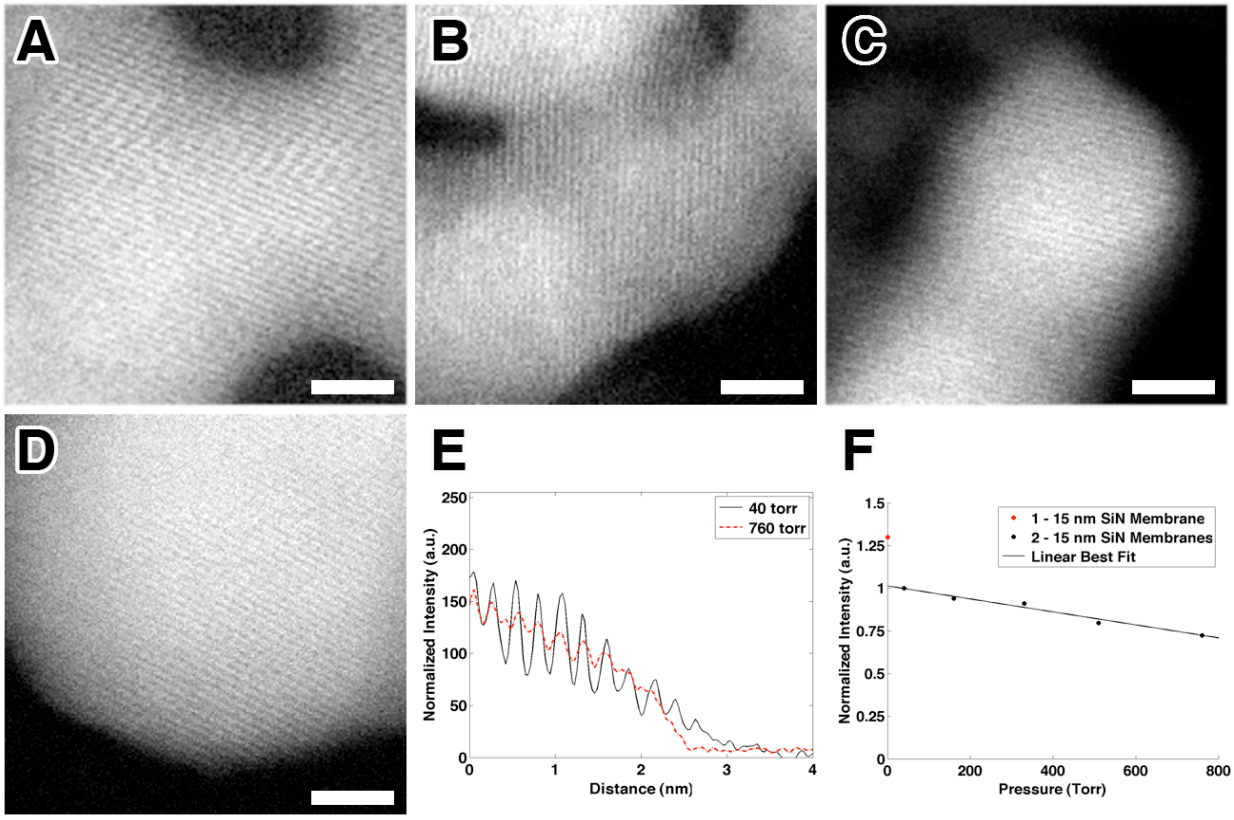

Figure 4: HAADF-STEM images showing lattice fringes for TiO_2 nanoparticles attached to silicon nitride membranes. A-D) Nanoparticles deposited between two 15 nm silicon nitride membranes inside the *in situ* environmental holder at 40, 163, 330 and 760 Torr O_2 gas respectively. Scale bars represent 3 nm. E) Plot showing line profiles for the nanoparticles depicted in A&D perpendicular to the 0.25 nm lattice fringes. F) Plot showing normalized IQ value of the 0.25 nm spots for 6 different gas pressures. The black circles indicate IQ values from particles between two membranes at pressures between 40 and 760 Torr. The red circle indicates the IQ value for a nanoparticle atop a single membrane and exposed to the high vacuum of the microscope (~10^{-7} Torr) for reference.